Scanning Electron Microscopy

Volume 1982
Number 1 *1982*

Article 12

1982

Energy and Atomic Number Dependence of Electron Depth-Dose and Lateral-Dose Function

Stephen P. Shea
University of Delaware

Electron Beam Interactions With Solids (Pp. 145-151)
SEM, Inc., AMF O'Hare (Chicago), IL 60666, U.S.A.

ENERGY AND ATOMIC NUMBER DEPENDENCE OF ELECTRON DEPTH-DOSE AND LATERAL-DOSE FUNCTIONS

Stephen P. Shea
Institute of Energy Conversion
University of Delaware
Newark, Delaware 19711
(302) 453-6251

ABSTRACT

A review of available Depth-Dose functions determined both experimentally and by Monte-Carlo simulation in a variety of materials reveals that, although there is general agreement as to the shape of the function, there is considerable disagreement concerning quantitative measures such as the range of the incident electrons and the position of the maximum of the Depth-Dose curve relative to the range. This finding is contrary to the typical assumption that the shape of the Depth-Dose curve is not dependent on the beam energy and only slightly dependent on the target material.

Current Address:
Solarex Corp.
1335 Piccard Dr.
Rockville, MD 20850
(301) 948-0202 x259

Keywords: Depth-Dose, Gaussian, Lateral Dose, Electron Beam-Induced Current, Poly-Methyl-Methacrylate, electron range, electron energy loss rate, range-energy relation.

INTRODUCTION

The Depth-Dose function, which describes the dissipation of electron beam energy with depth into an absorber, is important for modelling a number of electron beam-related effects. Electron emission from a target by backscattering or by secondary emission, x-ray production, Auger electron yields and cathodoluminescence (CL) efficiency are all dependent on the Depth-Dose function, as is the generation of electron beam-induced current (EBIC) in semi-conductor junction devices. For electron beam lithography, a knowledge of both the Depth-Dose function and the related Lateral-Dose function is necessary to optimize the exposure and development of the photoresist.

The Depth-Dose function dE/dx is defined as the energy loss per unit depth below the surface of the sample. A typical Depth-Dose profile is shown in Fig. 1. The curve rises to a maximum at a depth U_O and then descends nearly linearly before tailing off as the depth nears the maximum range. By extrapolating the linear part of the descending curve to zero, an alternate definition of the range is obtained. This is referred to as the Grün range (R_G) after the work of Grün [1957] who used this definition in measuring Depth-Dose functions in air. The Lateral-Dose function is defined similarly as the energy loss per unit distance from the axis of the electron beam, [Shea et al, 1978]. An experimental Lateral-Dose function measured in CdS is shown in Figure 2.

The work reported here was done in an effort to find the most appropriate form of the Depth-Dose function to use in a model for the EBIC response of a thin film heterojunction diode. Briefly, the form of the experiment is shown in Figure 3, and follows the design of Wu and Wittry [1978]. The electron beam strikes the target perpendicular to the plane of the collecting junction, and the induced current is measured as a function of the electron beam voltage. Wu and Wittry modelled the EBIC response of a Schottky barrier device in this experiment, and obtained experimental results for Si and for GaAs. Shea [1981] extended the theory to the more general case of a heterojunction diode, and applied these results to experiments on Cu_2S/CdS solar cells.

The EBIC response of a heterojunction device is determined by a number of variables in addition to the Depth-Dose function. These include the minority carrier diffusion lengths in the semiconductor layers; the recombination velocity of minority carriers at the top surface of the device; the recombination

LIST OF SYMBOLS

A	=	Atomic weight (gm/mole).
a, B, C	=	Constants
E; E_O; E_{EX}	=	Electron potential energy; Electron beam accelerating potential; Excitation energy, (eV).
e	=	Electron charge.
I	=	Mean Excitation Energy (Defined by Eq. 7) (eV).
k	=	Normalization constant defined by Eq. 9, (gm/cm²).
N_A	=	Avogadro's number.
P(Θ,E)	=	Probability density function for angular scattering of an electron of energy E through an angle Θ.
R; R_B; R_G, R_{MAX}	=	Electron range; Bohr-Bethe range; Grün range; Maximum range (cm).
s	=	Unit vector along the true (zig-zag) path of the primary electron (cm).
U_O	=	Depth at which the peak of the Depth-Dose function occurs.
V_e	=	Electron velocity (cm/sec).
Z	=	Atomic number.
ϱ	=	Density (gm/cm³).
Θ	=	Scattering angle.
ζ	=	Dimensionless energy defined as 1.1658 E/I.
m_O	=	Rest mass of electrons (gms).

velocity of carriers through interface states which exist at a heterojunction because of the slight lattice mismatch between the two semiconductor layers; the width of the depletion region; the presence and properties of an interfacial i-layer. Because of the complex dependence of the EBIC response on a number of variables, the experiment cannot be used to determine accurately the value of any given parameter, such as the minority carrier diffusion length, unless most of the other variables are known independently. Even if this is the case, reliable results depend on the accuracy of the model used for the Depth-Dose function, especially in materials with very short diffusion lengths.

The Depth-Dose function has been modelled empirically using several different approaches. Kyser and Wittry [1967], and Shea et al [1978] used a Gaussian distribution. Wu and Wittry [1978] used a Gaussian, modified by substracting an exponential term near the surface, and Everhart and Hoff [1978] used an orthogonal polynominal series to fit data from SiO_2. There have also been a number of determinations of Depth-Dose functions using Monte-Carlo simulations. References for some of this work are given in Table 1.

It is commonly assumed that the shape of the Depth-Dose curve is not a function of either the incident energy or the target material; that the Depth-Dose curve is universal when normalized to the electron range. In terms of Figure 2, the ratios R_G/R_{MAX} and U_O/R_{MAX} would be assumed constant.

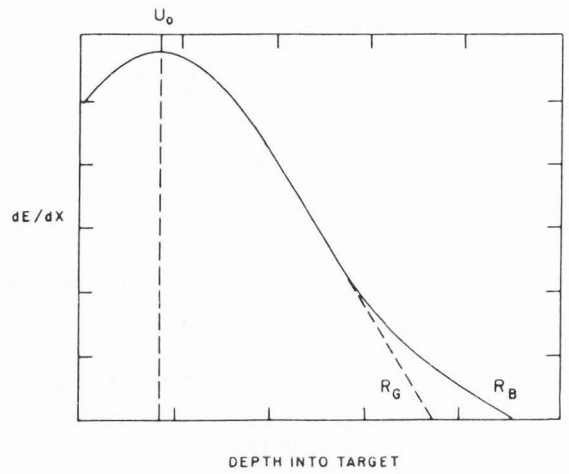

Fig. 1. Schematic Depth-Dose, $\phi(\varrho x)$ Function.

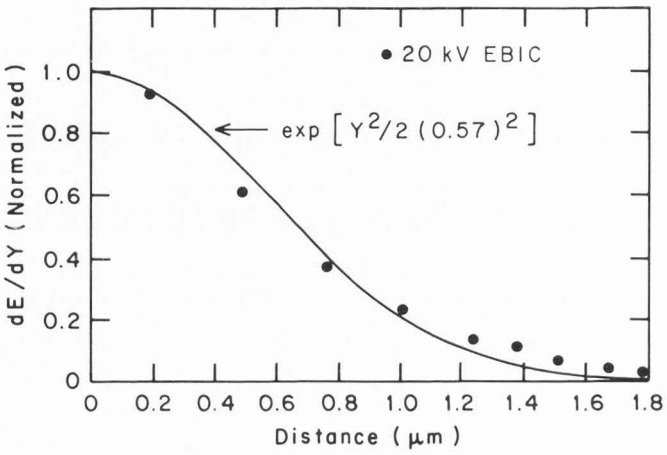

Fig. 2. Gaussian Least-Squares Fit to Lateral-Dose Function Measured in CdS.

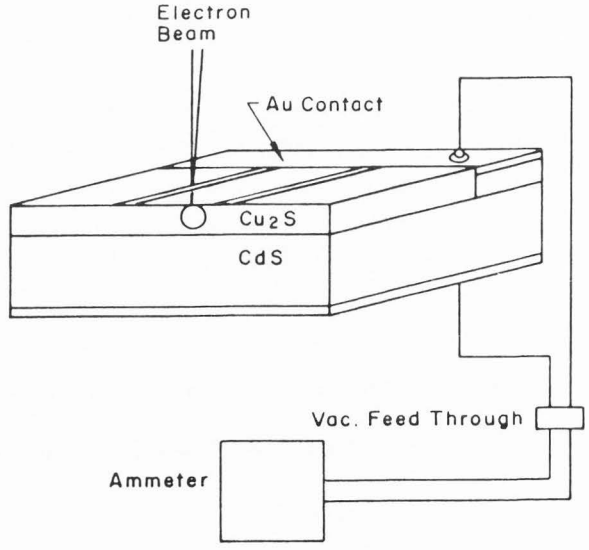

Fig. 3. Schematic of the Electron Beam-Induced Current (EBIC) Measurement in a Thin-Film Heterojunction Diode.

However, examination of published experimental results and of the Monte-Carlo simulations reveals that different values of these ratios have been found for different materials, although for a given material in a specific experiment the ratios appear to be constant. In addition, although published values of electron ranges are in qualitative agreement with a "universal" range-energy relationship proposed by Everhart and Hoff [1971], there is considerable scatter in the data. This makes it difficult to predict a value for the electron range in a given material with any certainty.

Review of Theory

Electron Range Rose [1966] discussed the rates of energy loss by an energetic electron to various processes. Figure 4, which was derived from Rose's work using parameters appropriate to CdS, is a plot of the rates of energy loss for plasmon generation, x-rays, polar optical phonons, and impact ionization. For kilovolt electrons, plasmon generation is the most rapid energy loss mechanism until the energy of the electron has been reduced by repeated collisions to the plasmon energy, which is in the range of 10 to 20 eV.

In order to calculate the total path length traversed by an electron incident on a given material, the assumption is usually made that all of the energy loss is to relatively small-energy, small-angle events. The large-angle scattering events are assumed to be perfectly elastic. The maximum range of the incident beam in the target will then be the distance travelled by a primary that avoids all large-angle events and moves along a nearly straight line until all of its energy has been dissipated. This distance is given by

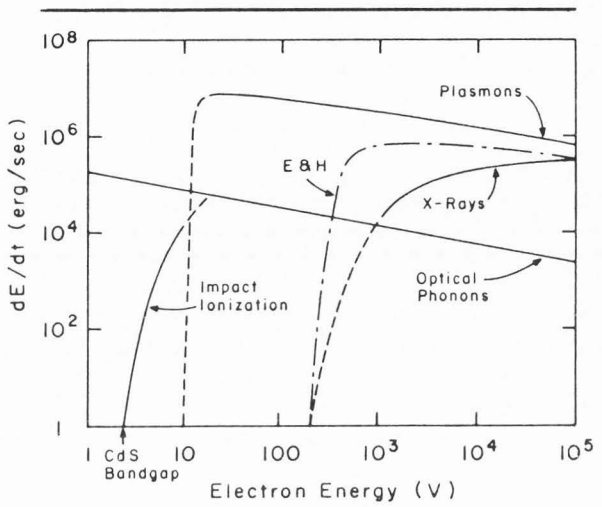

Fig. 4. Electron Energy Loss Rates to Various Mechanisms in CdS. [After Rose, 1966].

Table 1. Sources of Range-Energy Data from Experiment and Monte-Carlo Calculations

Reference	Material	Method	Range of Work	
			keV (Except as noted)	$\ln(\zeta_B)/Z$
Akamatsu et al (1981)	GaAs	Monte-Carlo M.C.	10-30	0.11-0.14
Ehrenberg and King (1963)	Styrene	Exp.	20-80	1.63-2.03
	$CaWO_4$	Exp.	20-80	0.22-0.28
	$CdWO_4$	Exp.	30-70	0.19-0.22
	KI	Exp.	20-60	0.10-0.14
	RbI	Exp.	10-50	0.07-0.11
	CsI	Exp.	20-80	0.07-0.10
Everhart and Hoff (1971)	SiO_2	Exp.	20	0.52
Grün (1957)	Air	Exp.	5-54	0.54-0.87
Reimer (1979)	C	M.C.	60	1.09
	Au	M.C.	60	0.06
Rosenzweig (1962)	Al	Exp.	0.61-1.16 MeV	0.65-0.69
Shimizu and Everhart (1972)	PMMA	M.C.	29	1.67
Shimizu and Everhart (1981)	P M M A	M.C.	20.7	1.58
Shimizu et al (1972)	Al	M.C.	15-30	0.36-0.41
	Cu	M.C.	15-30	0.14-0.16
	Au	M.C.	15-30	0.04-0.05
Spencer (1955)	Cu	Theory	25 keV-10 MeV	0.16-0.36

$$R = V_e E_o/(dE/dt) \quad (1)$$

Where $V_e = (2E_0/m_0)^{1/2}$, is the velocity of a (nonrelativistic) primary electron with initial energy E_0, and dE/dt is the time rate of energy loss to the fastest loss mechanism, in this case, to plasmons. For kilovolt electrons, $dE/dt = 10^6$ erg/sec from Figure 4, giving

$$R = 0.03E_o^{1.5}\ \mu m, \quad (2)$$

(for E_O in kV) as an appropriate expression for the total path length. The path length is about 1 μm for a 10 kV primary, and about 0.03μm for a 1 kV primary. This derivation assumes that dE/dt remains constant as the primary electron loses energy, which is a rather gross approximation to Figure 4, but is intended to give a rough idea of the expected range-energy relation.

A more accurate derivation of the range-energy relation may be obtained by considering the rate of energy loss by the primary electron per unit path length, dE/ds, where s is a unit vector in the direction of motion. This is given by Rose (after some algebra) as

$$\frac{dE}{ds} = B \cdot \frac{2N_A e^4}{E}\left(\frac{Z\varrho}{A}\right) \ln\left(\frac{4E}{E_{EX}}\right) \quad (3)$$

where N_A is Avogadro's number, Z, A and ϱ are the material's average atomic number, average atomic weight, and density, respectively, E is the remenant energy of the primary electron, and E_{EX} is the energy of the fastest energy loss mechanism. B is equal to 1 for the production of plasmons and of x-rays, and is less than 1 for optical phonons, the three loss mechanisms for which the equation is valid. Figure 4 was derived from this equation and the relationship

$$\frac{dE}{dt} = V_e \frac{dE}{ds} \quad (4)$$

Integration of along the path traversed by the primary electron gives a measure of the total range. The range calculated in this way will be designated the "Bohr-Bethe" range (R_B) following the usage of Everhart and Hoff [1971]. It is given by

$$R_B = \int_{E_0}^{0} dE/(dE/ds)\ cm. \quad (5)$$

Everhart and Hoff performed this integration using the formula

$$\frac{dE}{ds} = (2N_A e^4)\left(\frac{Z\varrho}{A}\right)\frac{1}{E}\ln\left(\frac{1.1658\ E_0}{I}\right) \quad (6)$$

where I is the "mean excitation energy" given empirically by

$$I = (9.76 + 58.8\ Z^{-1.19})\ Z\ eV \quad (7)$$

For CdS, I = 343. Using CdS as an example, dE/dt was calculated and plotted on Figure 4 for comparison to the curves calculated from Rose's paper. The Everhart and Hoff expression falls between the energy losses to plasmons and to x-rays.

Universal Range-Energy Relation

Everhart and Hoff have performed the integration indicated in Equation 5 after normalizing it in order to remove any variation due to the target material. By doing this, they have formulated the range-energy relation in a "universal" form. Application to any given material requires a knowledge of the average atomic weight, average atomic number, and the density. Their results are summarized below, followed by quantitative comparison of their work to a variety of experimental results by other authors.

Of the three bracketed terms in Equation 6 the first is constant, the second is primarily a function of the target density since Z/A is nearly constant, and the third depends on the electron energy and on Z. By defining a normalized energy $\zeta = 1.1658E/I$, and measuring distance along the path in units of ϱs in order to remove the density dependence, Equation 5 can be written as

$$R_B' = k \int_0^{\zeta(E_0)} \zeta\, d\zeta/d(\ln \zeta)\ gm/cm^2 \quad (8)$$

where

$$k = 9.4 \cdot 10^{-12}\ I^2(A/Z)\ gm/cm^2 \quad (9)$$

for A in grams and I in eV. By then letting

$$R_B = R_B'/k \quad (10)$$

where R_B is now dimensionless, a universal curve of normalized range versus normalized energy is obtained as shown in Figure 5. The approximate range-energy relation given by Equation 2 has been normalized and plotted on the same scale for comparison. Expressions of the form $R_B = C\zeta^a$ are given which closely approximate the function over three

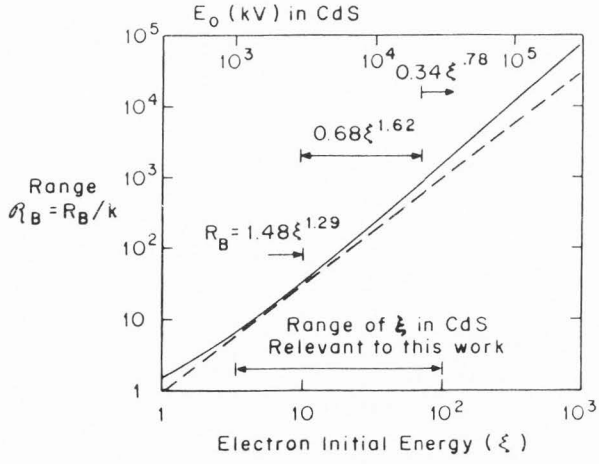

Fig. 5. Universal Range-Energy Relation of Everhart and Hoff (1971) Compared to Result Derived from the Simple Model Due to Rose (1966).

ranges of the incident energy. (Note that these three relationships are not quite identical to those used by Everhart and Hoff). The relationship

$$R_B = R_B \; k/\varrho \text{ cm} \tag{11}$$

is used to obtain the range in centimeters from the dimensionless range.

COMPARISON WITH EXPERIMENT

Since the Everhart and Hoff calculation for R_B is the maximum range an incident electron will travel if it is not deflected at all from its initial path, but experiences only a continuous energy loss, one would expect any experimental determination of the electron range to be less than this calculated value. A variety of experimental results from the literature, suitably normalized, are plotted in Figure 6 in comparison with the Everhart and Hoff curve. Several values calculated by Monte-Carlo methods are also shown. The sources for this figure are summarized in Table 1. The straight line in Figure 6 is a least square fit (LSF) to the experimental points. As expected, the experimental points lie almost entirely below the theoretical curve. The discrepancy between the theory and the experimental points is greater for higher electron energy. It is important to notice that, although the qualitative agreement with the theory can be reasonably characterized as good, and the LSF to the data is likewise good, an attempt to predict a given datum from the LSF curve can result in an inaccuracy of as much as 50% in many cases.

In addition to calculating the range-energy relation, Everhart and Hoff suggest an energy and atomic number dependence of the shape of the Depth-Dose function. For an incident electron at the surface of the sample, Everhart and Hoff give the ratio of the probability of angular scattering to fractional energy loss as

$$\frac{P(\Theta,E)}{(\Delta E/E)} = \frac{1}{32\pi} \cdot \frac{Z}{\ln \zeta_B} \sin^{-4}(\Theta/2) \tag{12}$$

where Θ is the scattering angle. They note that: "for a given scattering angle and energy, the large-angle scattering per unit fractional energy loss increases more rapidly than linearly with Z. Thus the path through the material will be more zigzagged at highest Z, and the peak of the energy dissipation will be expected to move toward the surface as Z increases." This also implies that the ratio R_G/R_{MAX} should decrease with increasing Z. Furthermore, both R_G/R_{MAX} and U_0/R_{MAX} will depend on the energy of the primary electron through ζ_B, although this will be a weak dependence for higher energies because ζ_B enters Equation 12 logarithmically. These ratios should therefore also increase with increasing electron energy.

Figures 7 and 8 are, respectively, plots of R_G and U_0 taken from the same sources used for Figure 6. Again, the straight lines are the best fit to the experimental points. Comparison of these three figures shows that the ratios R_G/R_{MAX} and U_0/R_{MAX} do tend to increase with increasing beam energy, although the scatter in the data is greater than that for the R_{MAX} data shown in Figure 6.

A different way of organizing the data is suggested by Equation 12. If the ratios R_G/R_{MAX} and U_0/R_{MAX} are plotted

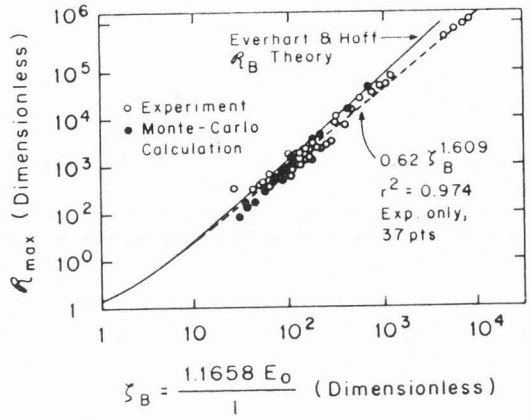

Fig. 6. Comparison of Experimental and Monte-Carlo Maximum Ranges with the Universal Curve.

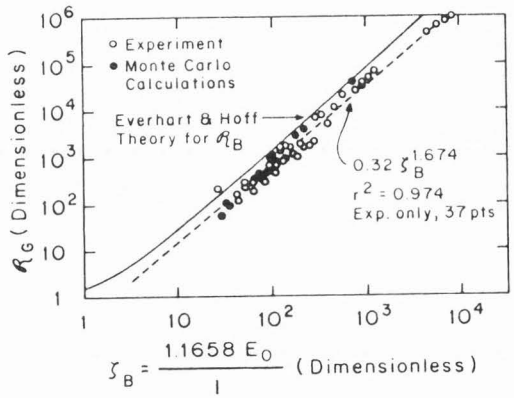

Fig. 7. Comparison of Experimental and Monte-Carlo Grün Ranges with the Universal Curve.

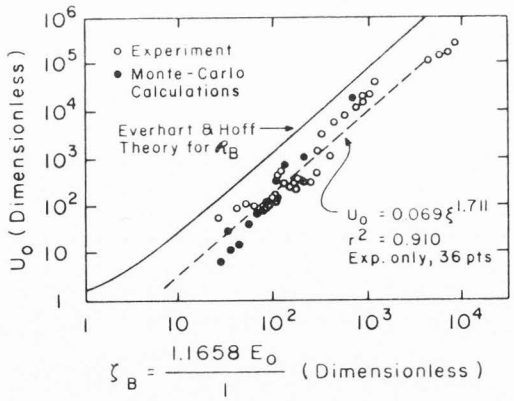

Fig. 8. Comparison of Experimental and Monte-Carlo Depth-Dose Maxima with the Universal Curve.

against $\ln \zeta_B/Z$, then the effects of both electron energy and atomic number will be represented (although there is, of course, already a weak atomic number dependence in the value ζ_B). Figures 9 and 10 show the data from Figures 7 and 8 replotted in this way. Average values are plotted over the range of $\ln \zeta_B/Z$ used in a particular experiment. The trend in both figures is in the anticipated direction, with R_G/R_{MAX} and U_0/R_{MAX} generally increasing with increasing energy or decreasing atomic number. However, the scatter is still significant, even for the averaged values.

Figures 9 and 10 can be divided into roughly two regions. For $\ln \zeta_B/Z \ll 1$, the effect of large angle scattering will be large relative to energy loss. The direction of the incident electrons will be more quickly randomized in this region and the resulting Depth-Dose and Lateral-Dose functions will be expected to be nearly Gaussian in form. A Gaussian LSF to a Lateral-Dose function measured in CdS using an EBIC technique is shown in Figure 2 (Beam Voltage = 2 kV; $\ln \zeta_B/Z$ = 0.13). The fit is reasonable in this case. However, for $\ln \zeta_B/Z > 1$, large angle scattering will be less effective in randomizing the direction of the primaries, and the energy dissipation functions should not be expected to be Gaussian. Depth-Dose and Lateral-Dose functions derived from the Monte-Carlo data of Shimizu and Everhart [1981] for poly-methylmethacrylate (PMMA), (Beam Voltage = 20.7 kV; $\ln \zeta_B/Z$ = 1.58) are, in fact, not adequately represented by Gaussian functions.

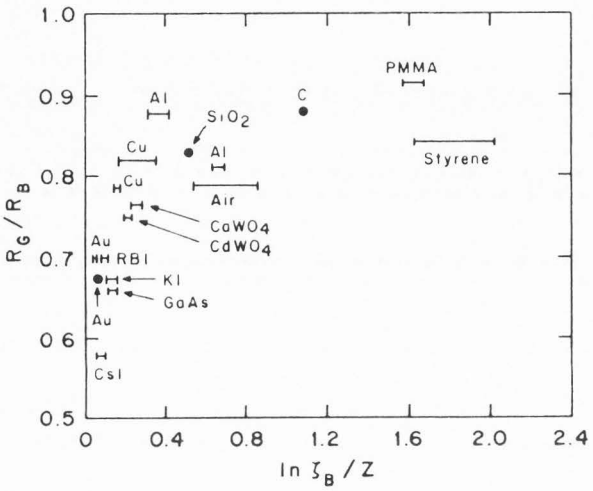

Fig. 9. Ratio of Grün Range to Maximum Range for various Materials from Experiment and Monte-Carlo Calculation (See Table 1 for References).

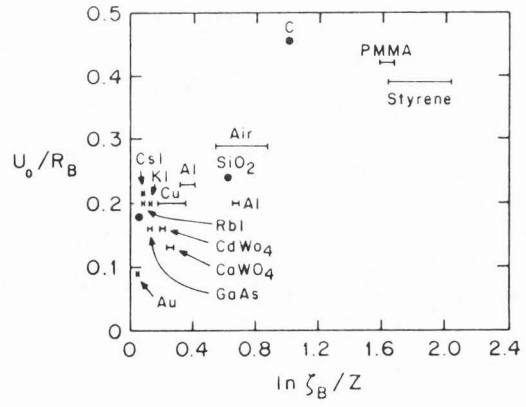

Fig. 10. Ratio of Depth-Dose Maximum Range for Various Materials.

CONCLUSIONS

A review of available measured Depth-Dose function was made, and a quantitative comparison of measured electron ranges made with the theory of Everhart and Hoff. Although the general agreement was reasonable, the wide scatter in the data, and even between Monte-Carlo calculations suggests that apriori calculations of the electron range may differ significantly from experimental determinations. In addition, consideration of the relative effects of large angle scattering and energy loss indicates that empirical models for the Depth-Dose function derived for such materials as GaAs, CdS and SiO_2 are not appropriate for low atomic number materials such as poly-styrene or PMMA.

ACKNOWLEDGEMENT

The author would like to thank P.J. Warter, Jr. of the Department of Electrical Engineering, and J.D. Meakin of the Institute of Energy Conversion, both at the University of Delaware, for their contributions. This work was supported by the Department of Energy through contracts with the Institute of Energy Conversion.

REFERENCES

1. Akamatsu B, Henoc J and Henoc P. (1981). Electron Beam-induced current in direct band-gap semiconductors. J. Appl. Phys. **52**, 7245-7250.

2. Ehrenberg W and King DEN. (1963). The Penetration of Electrons into Luminescent Materials. Proc. Phys. Soc., **81**, 751-766.

3. Everhart TE and Hoff PH. (1971). Determination of Kilovolt Energy Dissipation vs. Penetration Distance in Solid Materials. J. Appl. Phys. **42**(13), 5837-5846.

4. Grün Von AE. (1957). Lumineszenz-Photometrische Messungen der Energieabsorption im Strahlungsfeld von Electronenquellen Eindimensionaler Fall in Luft (Photometric Luminescence Measurements of the Energy Absorption by Ionization for One-Dimensional Electron Stopping Paths in Air). Zeitschrift für Naturforschung. **2**, 89-95.

5. Kyser DF and Wittry DB. (1967). Spatial Distribution of Excess Carriers in Electron Beam Excited Semiconductors. Proc. IEEE, Proc. Letters, IEEE, Inc., N.Y., May, 733-734.

6. Rose A. (1966). The Acoustoelectric Effects and the Energy Losses by Hot Electrons—Parts I-II. RCA Review, March, 98-131 and December, 600-631.

7. Reimer L. (1979). Electron-Specimen Interactions. Scanning Electron Microsc. 1979; 11:111-124.

8. Rosenzweig W. (1962). Diffusion Length Measurement by Means of Ionizing Radiation. Bell System Tech. J. **41**, 1573-1588.

9. Shea SP, Partain LD and Warter PJ. (1978). Resolution Limits of the EBIC Technique in the Determination of Diffusion Lengths in Semiconductors. Scanning Electron Microsc. 1978; I:435-443.

10. Shea SP. (1981). Electron Beam Induced Current (EBIC) measurement of heat treated polycrystalline cuprous sulfide/cadmium sulfide solar cells. Ph.D. dissertation, University of Delaware, Newark.

11. Shimizu R and Everhart TE. (1972). Monte Carlo simulation of the Energy Dissipation of an Electron Beam in an Organic Specimen. OPTIK. **36**(1), 59-65.

12. Shimizu R and Everhart TE. (1981). Lateral spreads of energy dissipation profiles of 20kV electrons in polymethylmethacrylate: Functional representation and its application to proximity effect. J. Appl. Phys. **52**(3), 1473-1477.

13. Shimizu R, Ikuta T and Murata K. (1972). The Monte Carlo technique as applied to the fundamentals of EPMA and SEM. J. Appl. Phys. **43**(10), 4233-4249.

14. Spencer LV. (1955). Theory of Electron Penetration. Phys. Rev. **98**(6), 1597-1615.

15. Wu CJ and Wittry DB. (1978). Investigation of Minority-carrier Diffusion Lengths by Electron Bombardment of Schottky Barriers. J. Appl. Phys. **49**(5), 2827-2835.